Genomics 115 (2023) 110604

Contents lists available at ScienceDirect

Genomics

journal homepage: www.elsevier.com/locate/ygeno

Dynamics of RNA m^{5}C modification during brain development

Zachary Johnson [a,b,1], Xiguang Xu [a,c,d,1], Yu Lin [a,d], Hehuang Xie [a,b,c,d,e,f,*]

[a] Epigenomics and Computational Biology Lab, Fralin Life Sciences Institute, Virginia Tech, Blacksburg, VA 24061, USA
[b] Genetics, Bioinformatics and Computational Biology Program, Virginia Tech, Blacksburg, VA 24061, USA
[c] Department of Biological Sciences, College of Science, Virginia Tech, Blacksburg, VA 24061, USA
[d] Department of Biomedical Sciences and Pathobiology, Virginia-Maryland College of Veterinary Medicine, Virginia Tech, Blacksburg, VA 24061, USA
[e] Translational Biology, Medicine, and Health Program, Virginia Tech, Blacksburg, VA 24061, USA
[f] School of Neuroscience, Virginia Tech, Blacksburg, VA 24061, USA

ARTICLE INFO

Keywords:
Brain development
Neuron
Neural stem cell
RNA cytosine methylation
RNA bisulfite sequencing
RNA-seq

ABSTRACT

Post-transcriptional RNA modifications have been recognized as key regulators of neuronal differentiation and synapse development in the mammalian brain. While distinct sets of 5-methylcytosine (m^{5}C) modified mRNAs have been detected in neuronal cells and brain tissues, no study has been performed to characterize methylated mRNA profiles in the developing brain. Here, together with regular RNA-seq, we performed transcriptome-wide bisulfite sequencing to compare RNA cytosine methylation patterns in neural stem cells (NSCs), cortical neuronal cultures, and brain tissues at three postnatal stages. Among 501 m^{5}C sites identified, approximately 6% are consistently methylated across all five conditions. Compared to m^{5}C sites identified in NSCs, 96% of them were hypermethylated in neurons and enriched for genes involved in positive transcriptional regulation and axon extension. In addition, brains at the early postnatal stage demonstrated substantial changes in both RNA cytosine methylation and gene expression of RNA cytosine methylation readers, writers, and erasers. Furthermore, differentially methylated transcripts were significantly enriched for genes regulating synaptic plasticity. Altogether, this study provides a brain epitranscriptomic dataset as a new resource and lays the foundation for further investigations into the role of RNA cytosine methylation during brain development.

1. Introduction

Over the past decade, epitranscriptomics has emerged as a new field to study the post-transcriptional modifications of RNA bases on a transcriptome-wide scale [1]. Among the over 170 kinds of RNA modifications, RNA cytosine methylation (m^{5}C) has gradually been recognized as an important form regulating RNA metabolism. The m^{5}C modification on tRNAs regulates tRNA stability and protein translation [2], while cytosine methylation on rRNAs coordinates mitochondrial assembly and translation activity [3,4]. Despite their lower abundance, maternally derived m^{5}C-mRNAs are essential for embryonic development during the maternal-to-zygotic transition [5] and ablation of maternal m^{5}C-mRNAs results in developmental delay and embryonic defects [6]. Cytosine methylation on mammalian mRNAs is primarily catalyzed by NOP2/Sun RNA Methyltransferase 2 (NSUN2) [7,8] and is removed *via* m^{5}C oxidation by the Ten Eleven Translocation enzymes [9,10]. At DNA damage sites, the RNA methyltransferase, TRNA Aspartic Acid Methyltransferase 1 (TRDMT1), is recruited to introduce m^{5}C to mRNA in the form of DNA:RNA hybrids [11]. The methylated RNA in such hybrids was recognized by the m^{5}C readers RAD51/52 [11]. Another m^{5}C binding protein, Aly/REF Export Factor (ALYREF), mediates the export of methylated mRNAs from the nucleus to the cytoplasm [7]. mRNAs carrying m^{5}C sites can also be recognized by the Y-box binding protein 1 (YBX1), which recruits the poly(A) binding protein cytoplasmic 1a (PABPC1A) to achieve stabilization of methylated mRNAs [12].

Accumulating literature emphasizes the important roles of RNA post-transcriptional modifications in brain development and function. In neuronal stems cells, the loss of RNA methyltransferase NSUN2 results in decreased m^{5}C-tRNA levels, leading to aggregation of tRNA fragments, activation of a cellular stress response, and impairment of neuronal stem cell differentiation [13,14]. In mouse models, NSUN2 loss inhibits the neurogenesis of upper-layer cortical neurons inducing microcephaly and motor defects [13,15]. Later, targeted knockout of NSUN2 in the mouse

* Corresponding author at: Epigenomics and Computational Biology Lab, Fralin Life Sciences Institute, Virginia Tech, Blacksburg, VA 24061, USA.
E-mail address: davidxie@vt.edu (H. Xie).
[1] These authors contributed equally to this work.

https://doi.org/10.1016/j.ygeno.2023.110604
Received 19 October 2022; Received in revised form 26 February 2023; Accepted 3 March 2023
Available online 6 March 2023

prefrontal cortex was shown to have reduced levels of m^5C-tRNA and resulted in the disruption of neuronal synaptic signaling patterns and behavior [16]. Although the influence of NSUN2 loss on mRNA methylation remains unclear, methylated mRNAs in brain tissue were found to be enriched for genes involved in ion transport and synapse function [17]. In neuronal oxidative stress models, an elevation in mRNA methylation level was associated with the stress response and regulation of apoptosis [18]. In glioblastoma cells, methylated transcripts mediated by the m^5C writer NSUN6 were linked to the regulation of transcriptional and translational processes after alkylation treatment [19]. These findings indicate that m^5C-modified RNAs may influence brain cell differentiation and function. However, no previous study has attempted to characterize m^5C dynamics during mammalian brain development.

Brain development is driven by drastic transcriptome changes accompanied by an increase in cellular diversity and neuronal connectivity [20]. The expansion and migration of neuronal lineages occur at the pre-natal stage while post-natal brain development is characterized by active gliogenesis and rapid neuronal diversification [21,22]. Around postnatal day 17 (P17), the mouse brain enters a critical period of cortical plasticity that shapes neuronal circuits in response to early life experiences [23]. In this study, we performed RNA BS-seq to survey the landscape of mRNAs with methylated cytosines in the mouse brain at critical developmental time points, as well as neural stem cells and E16.5 cortical neuron cultures (Fig. 1A). In combination with bulk RNA-seq and single-cell RNA-seq data, we aimed to explore the links between the patterns of mRNA cytosine methylation and gene expression during brain development.

2. Materials and methods

2.1. Mice

C57BL/6 mice were maintained and bred in a 12-h light/dark cycle under standard pathogen-free conditions. Mouse brains were harvested at postnatal day 0, 17, and 6wk for total RNA extraction. Adult female mice were used for setting up timed pregnancy. Embryos were timed by checking virginal plugs daily in the morning. Positive plugs were designated as E0.5. The experiments were approved by the Institutional Animal Care and Use Committee (IACUC) of Virginia Tech.

2.2. Mouse neural stem cell (NSC) culture

Mouse NSCs were isolated from the subventricular zone (SVZ) of the lateral ventricles as described previously [24]. NSCs were seeded on poly-ornithine and laminin-coated plates. The culture media was prepared by mixing Dulbecco's Modified Eagle Medium (DMEM) and Ham's F12 media at 1:1 volume ratio, supplemented with 2% B27, 2 mmol/L L-

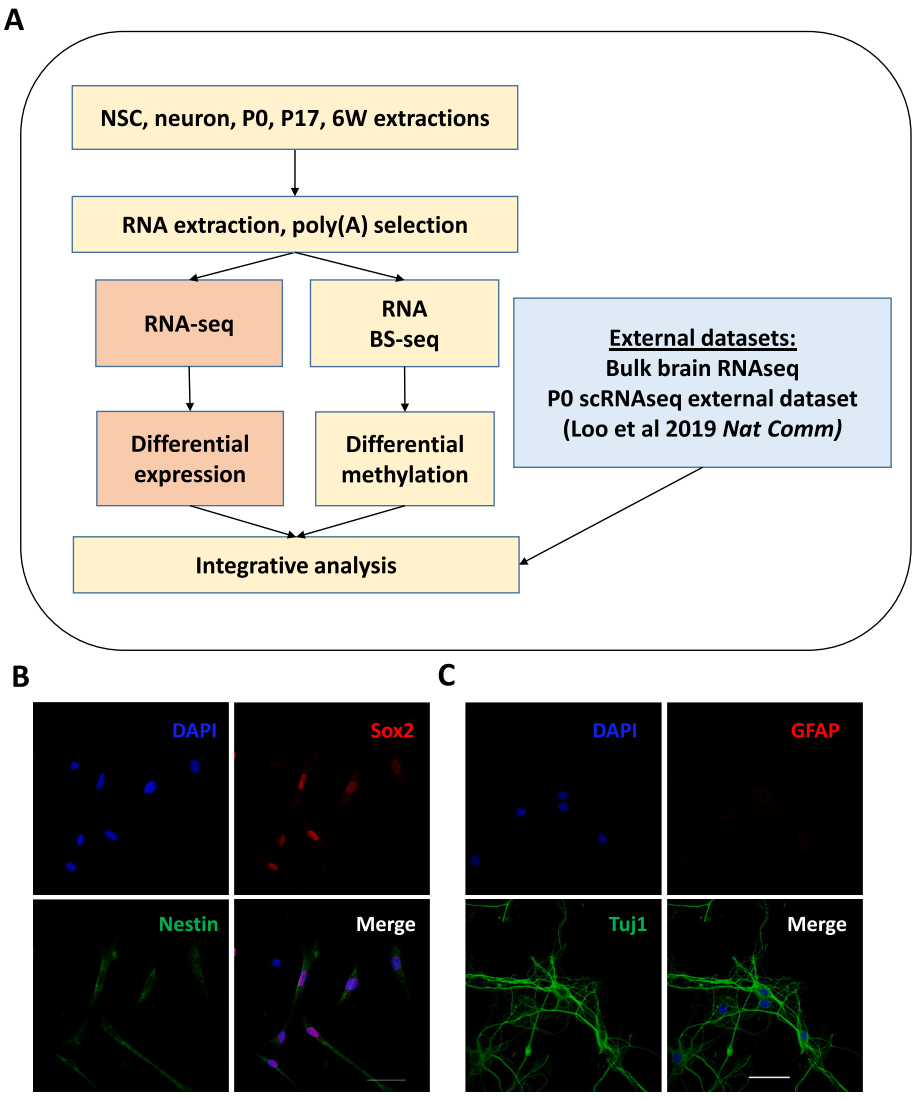

Fig. 1. Experimental Design. (A) Overall experimental design of this study. (B) Mouse neural stem cells (NSCs) were double stained with the neural progenitor markers Nestin (cytoplasmic, green) and Sox2 (nuclear, red); nuclei were counterstained with DAPI (blue). Scale bar: 50 μm. (C) E16.5 mouse cortical neuronal culture was double stained with the neuronal marker Tuj1 (green) and glial marker GFAP (red); nuclei were counterstained with DAPI (blue). Scale bar: 50 μm. (For interpretation of the references to color in this figure legend, the reader is referred to the web version of this article.)

glutamine, 1× penicillin-streptomycin, 20 ng/ml epidermal growth factor (EGF, PeproTech), and 20 ng/ml basic fibroblast growth factor (bFGF, PeproTech).

2.3. Primary mouse cortical neuronal culture

Primary mouse cortical neurons were prepared as previously described [25] with some modifications. Briefly, C57BL/6 E16.5 mouse embryos were micro-dissected for cortex tissues and the cortex tissues were dissociated into single-cell suspensions using the neural tissue dissociation kit (Cat# 130–092-628) according to manufacturer's instructions. After dissociation, neuronal cells were filtered through a 70-μm strainer (Falcon) and spun at 300 *g* for 10 min. The cell pellet was resuspended in neuronal culture medium (Neurobasal medium containing 2% B27 supplement (Invitrogen), 1% Glutamax (ThermoFisher), and 1% penicillin-streptomycin (ThermoFisher) and seeded on laminin and poly-ornithine coated 10-cm dishes. Neurons were grown *in vitro* for 7 days with fresh medium changed on Day 3 and Day 6.

2.4. Immunostaining

Immunostaining was performed as previously described [26]. Briefly, NSCs or E16.5 mouse cortical neurons were seeded onto an 8-well chamber. The neurons were fixed with 4% paraformaldehyde in phosphate buffered saline (PBS) for 15 min and permeabilized with 0.2% TritonX-100 in PBS for 10 min. After being blocked with 5% Normal Goat Serum (Thermo Fisher) at room temperature (RT) for 1 h, the cells were incubated with mouse anti-Nestin antibody (Millipore, MAB353) and rabbit anti-Sox2 antibody (Abcam, ab97959) for NSCs, or with mouse anti-Tuj1 antibody (Biolegend, 801,201) and rabbit anti-GFAP antibody (Sigma, HPA056030) for E16.5 cortical neurons at 4 °C overnight. Then, the cells were incubated with Cy3 conjugated anti-rabbit IgG (A10520, Invitrogen) and Alexa Fluor 488 conjugated anti-mouse IgG (A10680, Invitrogen) secondary antibodies at RT in darkness for 1 h. After washing 3 × 5 min with 1 × PBS, cells were mounted with DAPI-Fluoromount-G™ Clear Mounting Media (Southern Biotech, 010020). Fluorescent images were acquired using a confocal microscope.

2.5. RNA BS-seq library construction

RNA bisulfite conversion was performed as previously described [27] with minor modifications. Poly(A) RNA was first mixed with spiked-in Xef1 unmethylated RNA at a ratio of 0.5%. The spiked-in unmethylated mRNA was transcribed from the pTRI-Xef plasmid supplied by the MEGAscript™ T7 Transcription Kit (Invitorgen) according to manufacturer's instructions. RNA bisulfite conversion was performed with an initial denaturation at 95 °C for 1 min, followed by three cycles of 70 °C for 10 min and 64 °C for 45 min using the EZ RNA methylation Kit (Zymo Research). The bisulfite converted RNA was subjected to the stranded RNA-seq library construction procedure using the TruSeq Stranded mRNA Library Preparation Kit (Illumina). We modified the procedure to skip the RNA fragmentation step and supply both random and ACT random hexamers during the first strand cDNA synthesis.

2.6. RNA BS-seq data analysis

RNA BS-seq data analysis was performed as previously described [27]. Raw sequencing reads were trimmed at the 5′ and 3′ ends by 6 bp to account for methylation bias and then filtered for low quality bases and adaptor sequences. After the removal of reads with short lengths, clean reads were mapped to the mm10 genome (Ensembl v.79) using meRanGh [28]. To exclude partially unconverted reads, mapped reads were further filtered by removing reads with >3 "C"s ("G"s on the cDNA strand). Methylation calling was performed using meRanCall and subjected to a series of filters to reduce false positive signals [27]. In addition to the thresholds applied on the methylation level ($\geq$ 0.1) and read coverage ($\geq$ 20) of m^5C sites, additional filters were adopted including signal-to-noise ratio and the maximum number of m^5C sites detected in a read to reduce false positive methylation calling [27]. The C-coverage threshold ranging from 6 to 10 was determined using Gini Index [8]. High-confidence sites were defined as the m^5C sites passed all filters in both biological replicates.

2.7. Differential methylation analysis

Differential methylation analysis was performed using Fisher's exact test on high-confidence sites present in at least one sample. Benjamini-Hochberg *p*-value correction was used to correct for multiple comparisons, and sites with *p*-adjusted <0.05 were reported.

2.8. RNA-seq library construction

Stranded RNA-seq libraries were constructed using the TruSeq Stranded mRNA Library Preparation Kit (Illumina) following manufacturer's instructions. Briefly, after two rounds of poly(A) selection, the mRNA samples were fragmented and primed to synthesize first strand cDNA, followed by synthesis of the second strand cDNA. After Ampure XP bead purification, dA tailing was performed, and indexed adapters were ligated to both ends of the double-stranded cDNA. Adapter-ligated DNA fragments were enriched by PCR amplification for 12 cycles. After Ampure XP bead purification, the PCR products were size-selected with a range from 350 bp to 550 bp on 2% dye-free agarose gel using the pippin recovery system (Sage Science). The recovered libraries were sequenced on a Hiseq 4000 platform in the 150 bp paired end mode (Illumina).

2.9. RNA-seq data analysis

Trim Galore (version 0.6.5) was used to filter short reads, low quality reads, and trim adapter sequences from raw reads (https://www.bioinformatics.babraham.ac.uk/projects/trim_galore/). Clean reads were mapped to the mm10 genome and expression quantified using STAR (version 2.7.3a) [29]. Differentially expressed genes were identified using DESeq2 [30] using a fold change >1.5 and an adjusted *p*-value of 0.01 as cutoffs.

2.10. Gene ontology (GO) analysis

GO analysis was performed using DAVID (Database for Annotation, Visualization, and Integrated Discovery) [31]. The GO Direct terms, Biological Process (BP), cellular component (CC), and molecular function (MF) were identified. Significantly enriched terms were identified using Benjamini-Hochberg *p*-adjusted <0.05.

2.11. Clustering analysis

The z-score of bulk RNA-seq expression of transcript per million (TPM) and differentially methylated site methylation levels were used as input for clustering analysis. Clustering analysis was performed with the Python package sklearn's Agglometric Clustering. The 'complete' method was used with the number of clusters set to 5 for RNA-seq and RNA BS-seq datasets. Error bars represent the standard deviation of the z-score.

2.12. Availability of data and software

Data generated in this study were submitted to the NCBI Gene Expression Omnibus under accession number GSE207092. Analyses in this study was performed using the R v4.1.1, and Python 3.9.4 packages Biopython v1.78, matplotlib v3.3.4, Seaborn v0.11, and Pysam v0.16. The software package developed in this study is available in the GitHub

repository (https://github.com/zaustinj33/BrainDev).

3. Results

3.1. Identification of high-confidence m^{5}C sites in mouse NSCs, neurons, and brain tissues

To obtain RNA expression and m^{5}C epitranscriptome profiles during brain development, we performed RNA-seq and RNA BS-seq for NSCs (Fig. 1B), neurons in culture (Fig. 1C), and brain tissues isolated from postnatal day 0 (P0), postnatal day 17 (P17), and 6-week-old (6 W) mice. Two biological replicates were generated for each condition with a total of 10 libraries obtained for RNA-seq and RNA BS-seq (Table S1). Approximately 20 million paired-end reads were generated for each RNA-seq library and aligned to the mouse reference genome (mm10). For these libraries, the average percentage of sequences uniquely mapped to the reference was around 92%. The normalized gene expression level of the samples was provided (Table S2). Since methylation calling requires a much higher read depth compared with those of RNA-seq libraries, five times more sequences were generated for RNA BS-seq libraries (~100 million pair-end reads for each library). Sequencing reads derived from RNA BS-seq libraries were processed following the procedure described in our recent study [27]. In brief, bisulfite sequencing reads were first trimmed to remove adaptors and bases with low quality scores. After quality control, reads were mapped to the C2T converted mm10 genome. Around 85% of bisulfite sequencing reads were uniquely aligned (Table S1). Methylation calling was performed using meRanCall [28] and putative m^{5}C sites were subjected to a series of filters to reduce false positive signals [27].

A total of 2259 m^{5}C sites were identified from the ten RNA BS-seq libraries. Among these m^{5}C sites, 1758 sites passed all filters in one biological replicate but failed in the other; thus, these were denoted as "low-confidence" m^{5}C sites. The remaining 501 m^{5}C sites shared by both biological replicates were considered to be "high-confidence" in this study (Fig. 2A). The methylation levels of the high-confidence m^{5}C sites were highly correlated between the biological replicates and had Spearman *R* values between 0.82 and 0.92 (Fig. 2B). Notably, 76.4% of these sites had a methylation level lower than 0.3 (Fig. S1). This result was consistent with previous reports that only a small percentage of RNA copies are methylated for a given gene [8,27,32].

To explore the factors contributing to the level of confidence in methylation calling, we first compared methylation levels and read coverages of the high-confidence and low-confidence sites. Across five conditions, the high-confidence sites showed average methylation levels in the range of 0.18–0.21, while the low-confidence sites had average methylation levels in the range of 0.06–0.12 (Fig. 2C). The average read coverages for the high-confidence sites were between 109 and 227 reads per site, while the average for the low-confidence sites was only 24–48 reads per site (Fig. S2A&B). We next examined the relationship between read coverage and methylation level (Fig. S2C). A very weak positive correlation was observed between the methylation level and the read coverage for both high-confidence (Spearman $R < 0.19$) and low-confidence sites (Spearman $R < 0.08$). Altogether, the high-confidence m^{5}C sites tended to be found with a higher methylation level and

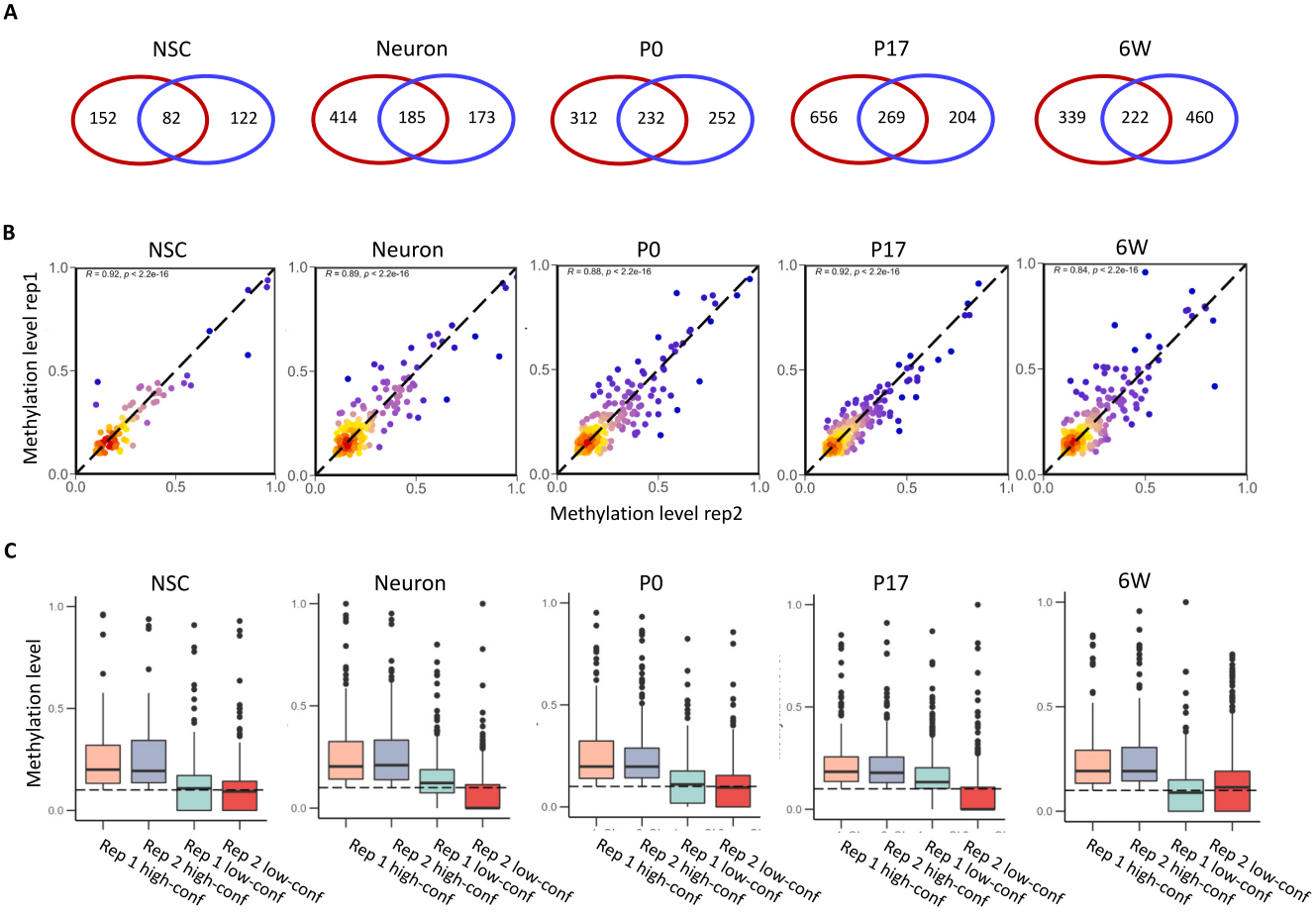

Fig. 2. Reproducibility of replicates among RNA BS-seq samples. (A) Overlap of m^{5}C sites identified between biological replicates. The red circle indicates replicate 1 and the blue circle indicates replicate 2. (B) Methylation correlation (Spearman's R) of the overlapping m5C sites between biological replicates. Color code indicates the density of sites, ranging from red (high density) to blue (low density). (C) Distribution of methylation levels for the overlapping and non-overlapping m^{5}C sites identified between biological replicates. (For interpretation of the references to color in this figure legend, the reader is referred to the web version of this article.)

more read coverage to enable them to survive all the stringent filters in both biological replicates.

Previous studies suggested that the process of library construction, the bisulfite conversion step in particular, could have a significant impact on methylation calling [8,27,32]. In this study, we generated both RNA-seq and RNA BS-seq data for the same pool of RNA samples. This enabled us to perform correlation analyses for the read coverage of each methylated transcript in the paired libraries for RNA-seq and RNA BS-seq. Interestingly, compared with the low-confidence sites, the high-confidence sites showed higher correlations in read coverage with or without bisulfite conversion, except for P17 brain samples in which the two correlations are similar (Fig. S3A). We further examined the average

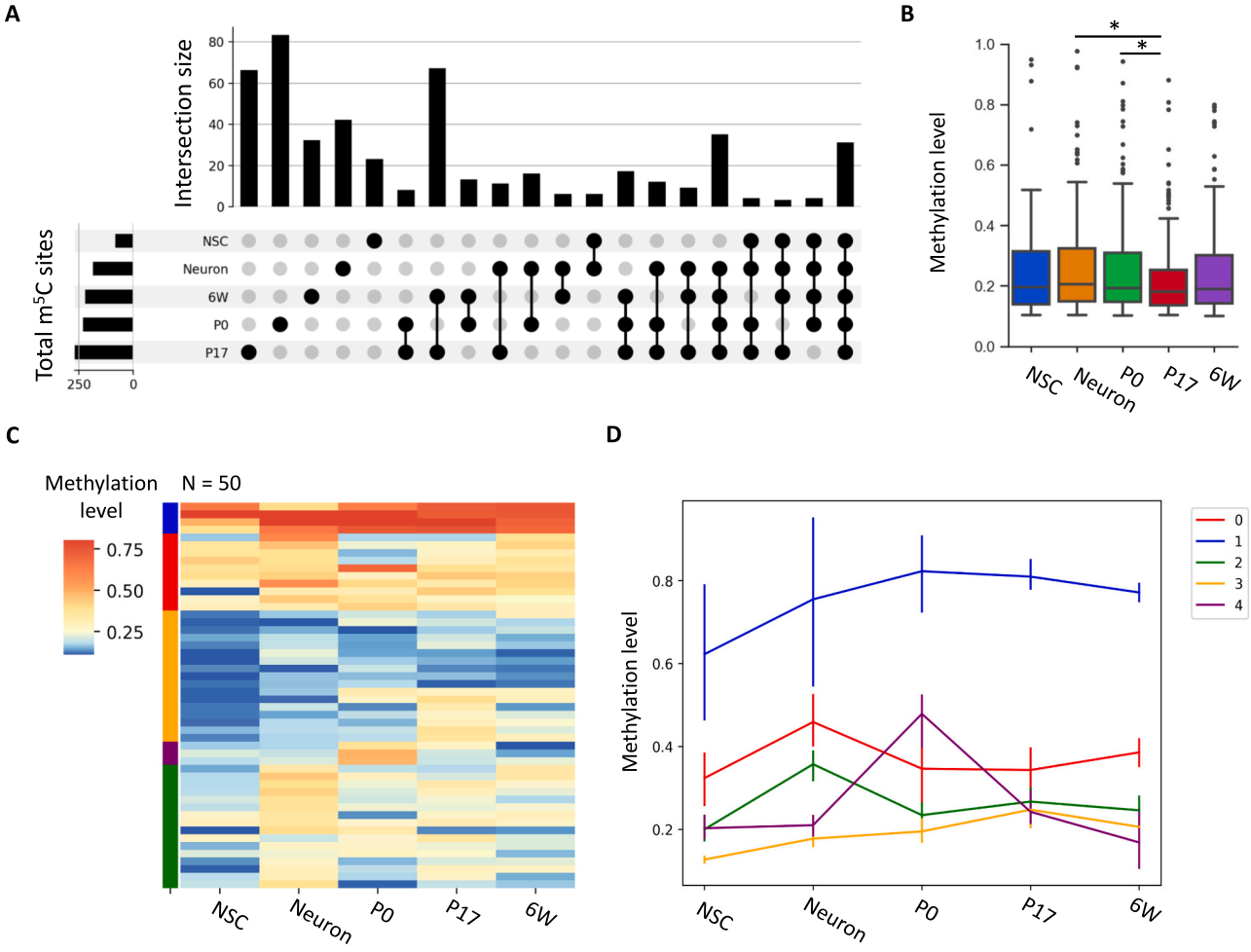

E

Term (Biological Process)	Genes
Group 1 (C1, C2, C3)	
response to insulin	PTPRN (C2), SRSF6 (C3), ZBED3 (C2)
synapse assembly	MYO6 (C3), CACNA1A (C2)
Group 2 (C0)	
positive regulation of transcription, DNA-templated	SMARCD3, MED24, WAC, FOXO3, RELA
chromatin organization	SMARCD3, WAC, RELA
tumor necrosis factor-mediated signaling pathway	FOXO3, RELA
positive regulation of pri-miRNA transcription from RNA polymerase II promoter	FOXO3, RELA
regulation of autophagy	RPTOR, WAC
stem cell population maintenance	MED24, MIAT
Group 3 (C4)	
proteasome-mediated ubiquitin-dependent protein catabolic process	BAG6, TRIM2

Fig. 3. Characteristics of high-confidence m^{5}C sites identified in NSCs, neuron, and brain samples. (A) High-confidence m^{5}C sites shared among conditions. (B) Methylation distribution of the high-confidence m^{5}C sites. Wilcoxon rank-sum test was performed to assess significance (*$p < 0.05$). (C) Clustering of m^{5}C sites according to methylation changes. (D) Average methylation levels of clusters identified in Fig. 3C. Bars indicate standard deviation. (C) and (D) share the same color code. (E) Gene ontology analysis of methylated transcripts.

length of methylated transcripts and the distribution of m^5C sites in transcripts. No significant difference in transcript length was detected for transcripts containing either high or low-confidence sites (Fig. S3B). The distribution of high-confidence sites was generally biased towards the 3'UTR of transcripts, in particular for the P17 brain samples (Fig. S3C). This result indicates that low-confidence sites tend to reside in a transcript sensitive to bisulfite treatment, but such sensitivity may not have a link with transcript length.

3.2. High-confidence m^5C sites differentially methylated in mouse NSCs, neurons, and brain tissues

We next focused on the 501 high-confidence sites to examine their sequence features and distribution across five conditions. Two common features of m^5C sites on mRNAs have been reported: 1) they often localize upstream of the translation initiation sites (TISs), and 2) a "GGG" motif is frequently observed downstream from the m^5C sites [8,27,32,33]. To determine the distribution of high-confidence m^5C sites along the transcripts, we binned the lengths of methylated transcripts into the 5′- untranslated region (5'UTR: bins 1–5), coding sequence (CDS: bins 6–28), and 3′- untranslated region (3'UTR: bins 19–46). Two density peaks surrounding TISs and an additional strong peak right before the termination of the coding region were observed for m^5C sites in all five conditions (Fig. S4A). A downstream "GGG" motif was determined for the high-confidence m^5C sites in all five conditions (Fig. S4B), which may serve as potential targets of the NSUN2 enzyme [8].

Out of 501 high-confidence m^5C sites, a total of 31 sites were identified as methylated in all conditions and 253 sites (50.8%) were shared by at least two conditions (Fig. 3A). Such a distribution indicates that at least some mRNAs are consistently methylated across multiple time points throughout brain development. Only 82 m^5C sites were identified in NSCs while the libraries derived from the three-stage brain tissues reported a similar number of high-confidence sites ranging from 222 to 269. In addition, m^5C sites in undifferentiated NSCs were largely overlapped with those in neurons and brain tissues. To determine the effect of sequencing depth on methylation calling, we calculated the yield of m^5C sites after normalizing to the number of total mapped reads for each library (Table S1). Despite more reads generated for NSC libraries, both NSC replicates yielded the fewest m^5C sites regardless of high-confidence or low-confidence. The methylation level of high-confidence sites reported in the P17 brain were significantly lower than sites reported in the P0 brain (Fig. 3B). These results suggested that the diversity of mRNA cytosine methylation may increase during brain cell specification.

Since brain development is accompanied with substantial changes in gene expression, we selected a set of 50 high-confidence m^5C sites that possessed at least 20× read coverage in all conditions. According to their average methylation levels, five clusters were identified with unique methylation patterns (Fig. 3C). The m^5C sites in three clusters had relatively consistent methylation levels throughout all conditions (at high, low, and medium methylation levels, respectively). Such stable methylation patterns suggest that cells from neural lineage may share a regulatory mechanism to control the methylation of a small set of transcripts. Cluster C0 and C4 showed high methylation levels in neurons and P0 brain samples, respectively (Fig. 3D). We further determined their associated transcripts for GO enrichment analysis. Interestingly, transcripts highly methylated in neuronal culture (cluster C0) were associated with transcription, chromatin organization, and stem cell maintenance (Fig. 3E). For instance, genes including *Foxo3, RelA,* and *Rptor* are important mediators of neuronal cell functions including reprogramming and differentiation [34] and synaptic formation [35].

3.3. Gene expression dynamics of methylated mRNAs, m^5C readers, writers, and erasers during brain development

We extended the analysis to identify differential methylation sites (DMSs) across five conditions. DMSs were defined as m^5C sites with a methylation difference ≥ 0.05 between two conditions and a *p*-adjusted value ≤ 0.05. Pairwise comparisons determined 83, 176, 62, and 172 DMS sites for NSCs *vs* neurons, P0 *vs* P17, P17 *vs* 6 W, and P0 *vs* 6 W, respectively (Fig. 4A). Interestingly, of the 83 DMSs identified between NSCs *vs* neurons, 96% showed increased methylation in neurons. Gene Ontology analyses indicated that differentially methylated sites in neurons compared to NSCs are significantly enriched for positive regulation of DNA-templated transcription, including RNA polymerase II transcription (Fig. 4B). The differentially methylated sites identified in postnatal brain tissues were significantly enriched for the regulation of GTPase activity and synaptic plasticity associated with brain development. For instance, the transcripts *Atxn1, Fgfr1,* and *Itsn1*, which are known to be critical for brain development, were found to be hypomethylated in the P0 brain.

To examine the relationship between RNA cytosine methylation and gene expression, we performed differential expression analysis of sample-matched RNA-seq libraries. These differentially expressed genes (DEGs) were defined as transcripts with an expression difference $\geq$ 1.5-fold between two conditions and a *p*-adjusted value ≤ 0.01. The majority of transcripts carrying DMSs were not differentially expressed between P17 and 6 W (Fig. 4C), while a number of genes showed significant changes in both gene expression and RNA methylation during early brain development. A moderate positive correlation ($R = 0.337$ in NSCs *vs* neurons) was observed between the changes in gene expression and RNA methylation (Fig. 4D). As aforementioned, transcripts carrying m^5C sites tend to have a higher methylation level in neurons compared to those in NSCs. Of those differentially methylated transcripts, 52.3% exhibited an increased expression level in neurons. Notably in neuronal samples, the transcript *Psd,* which codes for a Plekstrin homology and SEC7 domain-containing protein, was over-expressed and hypermethylated. SEC7 domains were conserved throughout many proteins and served to catalyze the guanine nucleotide exchange factor initiating the formation of vesicle coating [36]. However, both positive and negative correlations between gene expression and RNA cytosine methylation were observed for pairwise comparisons of NSCs *vs* neurons, P0 *vs* P17, and P0 *vs* 6 W. For instance, the differentially methylated transcripts *Csf1r* and *Endod1*, which were hyper-methylated and under-expressed in the P0 brain, are markers for microglia and endothelial cell types, suggesting cell-type specific methylation of transcripts. Conversely, two transcripts, *Map6* and *Sdc3*, were consistently hypermethylated and over-expressed in P0 samples compared to P17 and 6 W samples. *Map6* infers structural stability in developing neuronal microtubules, promoting interconnectivity and signaling [37,38], while *Sdc3* is a well-known mediator of neuronal lineage, promoting neuronal migration and synapse formation [39,40]. This result indicated that the regulation of RNA cytosine methylation and gene expression may be cell-type specific and is positively correlated for some transcripts.

Recently, significantly increased understanding has been gained about the writers, readers, and erasers of m^5C in mRNAs [41–44]. To examine the expression patterns of these factors, we first identified the top 1000 variably expressed genes in our RNA-seq dataset and performed clustering analysis (Fig. 5A). Not surprisingly, NSCs showed distinct gene expression profiles from other samples. We further checked the expression profiles of the factors regulating RNA cytosine methylation. It showed highly dynamic expression patterns during neural cell specification and postnatal brain development (Fig. 5B). In the comparison between NSCs and neurons, it showed that NSUN2 and YBX1 are highly expressed in both, while NSUN4, ALYREF, and FMR1 are highly expressed in NSCs, TET1 and TET3 are highly expressed in neurons (Fig. 5B). In the comparison among the three postnatal stages (P0, P17 and 6 W), it underwent clear downregulation trend, with the P0 brain

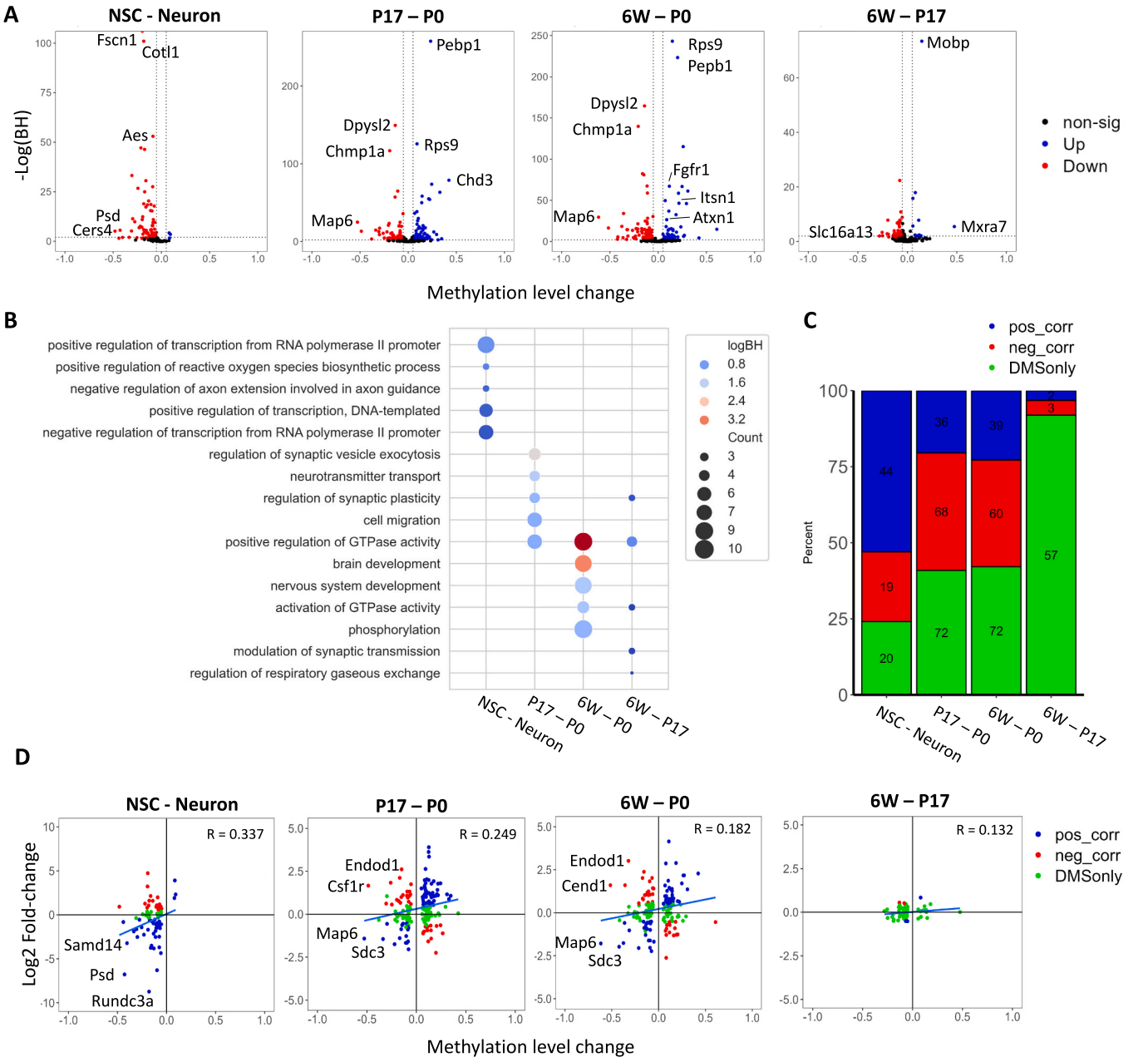

Fig. 4. Methylation dynamics throughout brain development. (A) Differential methylation analysis of neuron and brain samples. Blue and red points represent significantly hyper and hypo methylated transcripts, respectively. Significance was determined using Fisher exact test followed by Benjamini-Hochberg correction for multiple comparison ($p < 0.05$), requiring a minimum difference of 0.05 in methylation. (B) Gene Ontology analysis of differentially methylated transcripts identified in (A). (C) Correlation analysis of changes in RNA expression and methylation for transcripts carrying differentially methylated sites. Blue and red bars represent positive and negative correlation between methylation level difference and expression fold-change, respectively. Green bars represent transcripts without expression fold-changes above 2 and *p*-adjusted <0.01. (D) Dot plot representation of transcripts to indicate the changes in methylation and expression. Overall correlation was determined using Spearman's R. Transcripts with methylation difference over 0.3 are notated. (For interpretation of the references to color in this figure legend, the reader is referred to the web version of this article.)

displayed the highest expression for most m^5C readers/writers/erasers. Except that NSUN4 and RAD52 showed increasing upregulation during postnatal brain development (Fig. 5B). We further performed pairwise comparisons to determine the transitions in gene expression (Fig. 5C). With the cutoff of fold change >1.5 and an adjusted *p*-value <0.01, 9501 DEGs were identified in between NSCs and neurons, 6672 DEGs and 6997 DEGs were identified in the comparison P17 *vs* P0, and 6 W *vs* P0, respectively, while only 430 DEGs were identified in the comparison between 6 W and P17 (Fig. 5C). Consistent with the transcriptome-wide differences among the four comparisons, the 6 W *vs* P17 comparison yielded the fewest differentially expressed factors related to RNA m^5C regulation (Fig. 5D). This suggests that m^5C regulation is highly dynamic during early postnatal brain development and may reach homeostasis throughout the maturation process.

3.4. Differentially methylated transcripts have cell type-specific expression patterns and are temporally regulated in developing brains

During brain cell specification, more m^5C sites (Fig. 3A) and increased methylation (Fig. 3B) were observed in differentiated neurons and maturing brains. This inspired us to further examine the temporal expression patterns of differentially methylated transcripts using bulk

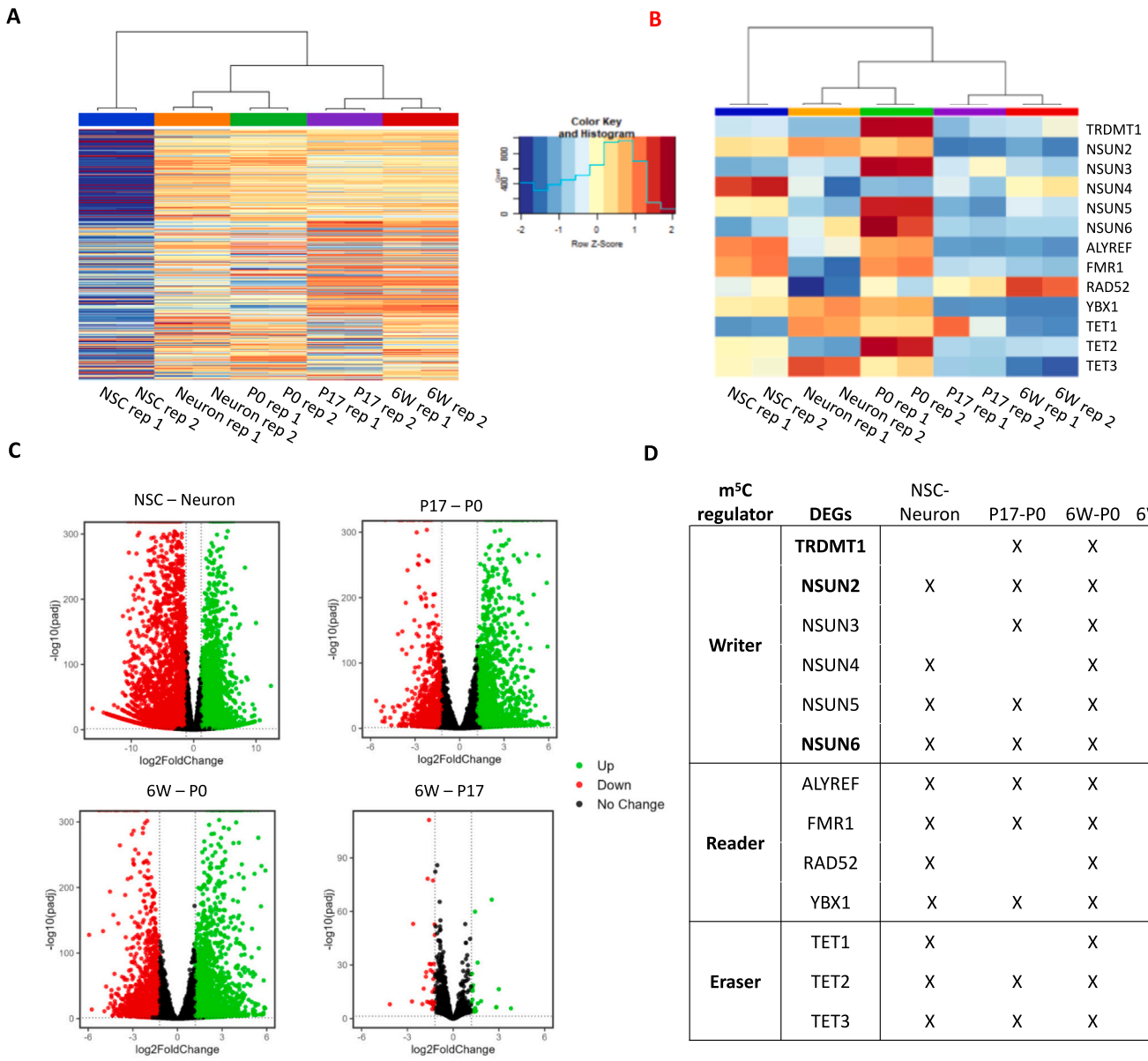

D

m^{5}C regulator	DEGs	NSC-Neuron	P17-P0	6W-P0	6W-P17
Writer	**TRDMT1**		X	X	
	NSUN2	X	X	X	
	NSUN3		X	X	
	NSUN4	X		X	
	NSUN5	X	X	X	X
	NSUN6	X	X	X	
Reader	ALYREF	X	X	X	
	FMR1	X	X	X	
	RAD52	X		X	
	YBX1	X	X	X	X
Eraser	TET1	X		X	X
	TET2	X	X	X	
	TET3	X	X	X	X

Fig. 5. Differentially expressed transcripts among NSCs, neurons, and brain tissues. (A) TPM expression values of the top 200 differentially expressed genes identified in each comparison (NSC *vs* Neuron, P0 *vs* P17, P0 *vs* 6 W, and P17 *vs* 6 W). TPM values and density are displayed in the figure legend. (B) TPM expression values of m^{5}C reader, writer, and eraser enzymes. (C) Volcano plots showing differentially expressed transcripts identified in each comparison (NSC *vs* Neuron, P0 *vs* P17, P0 *vs* 6 W, and P17 *vs* 6 W). Overexpressed genes are highlighted in green while under expressed genes are highlighted in red (fold-change ≥2, *p*-adjusted ≤0.01). (D) Dynamic expression of m^{5}C-RNA readers, writers, and erasers. In pair-wise comparisons, differentially expressed transcripts are denoted with an "X". (For interpretation of the references to color in this figure legend, the reader is referred to the web version of this article.)

RNA-seq data publicly available for mouse embryonic/postnatal brain tissues including different neuronal subsets. We focused on 42 differentially methylated transcripts identified in the RNA BS-seq datasets, which also showed expression fold-change >2 across the five RNA-seq conditions (Fig. 6A). According to their expression profiles in bulk RNA-seq, four distinct clusters were identified (Fig. 6B). Cluster 1 and cluster 3 were characterized with high expression levels in the adult brain and newborn brain, respectively. Of the Cluster 1 transcripts, *Endod1, Wbp2,* and *Rapgef4* were highly expressed in the mature 22-month-old brain samples and were found to be both over-expressed and hyper-methylated in our 6 W brain samples compared to the P0 brain. ENDOD1, an endothelial marker, was found in a previous study to have high expression in the cerebral cortex and hippocampus, while WW domain binding protein 2 (WBP2) and Rap guanine nucleotide exchange factor 4 (RAPGEF4) were mainly localized to the cerebral cortex [45,46]. WBP2 is a transcriptional co-activator of estrogen receptor α (ESR1), of which mutations induce abnormal glutamatergic synapse development [47].

Methylated transcripts in cluster 2 showed highest expression level in neurons. To further examine the expression patterns of these methylated transcripts, we integrated the epitranscriptome profiles generated in this study with an scRNA-seq dataset recently published for the P0 cortex [22] (Fig. 6C). Previous studies reported that the methylation of tRNAs is essential for proper development of cortical layers [13,15]. Intriguingly, scRNA-seq data also suggested that some genes with abundant neuronal expression were associated with a relatively high level of mRNA methylation (Fig. 6D). In neurons, the *Psd*, *Rundc3a*, and *Smarcd3* transcripts were hyper-methylated, and their expressions were also broadly enriched for many neuronal subpopulations in cortical layers I-VI, interneurons 1–3, and striatal inhibitor neurons 1 and 2. For

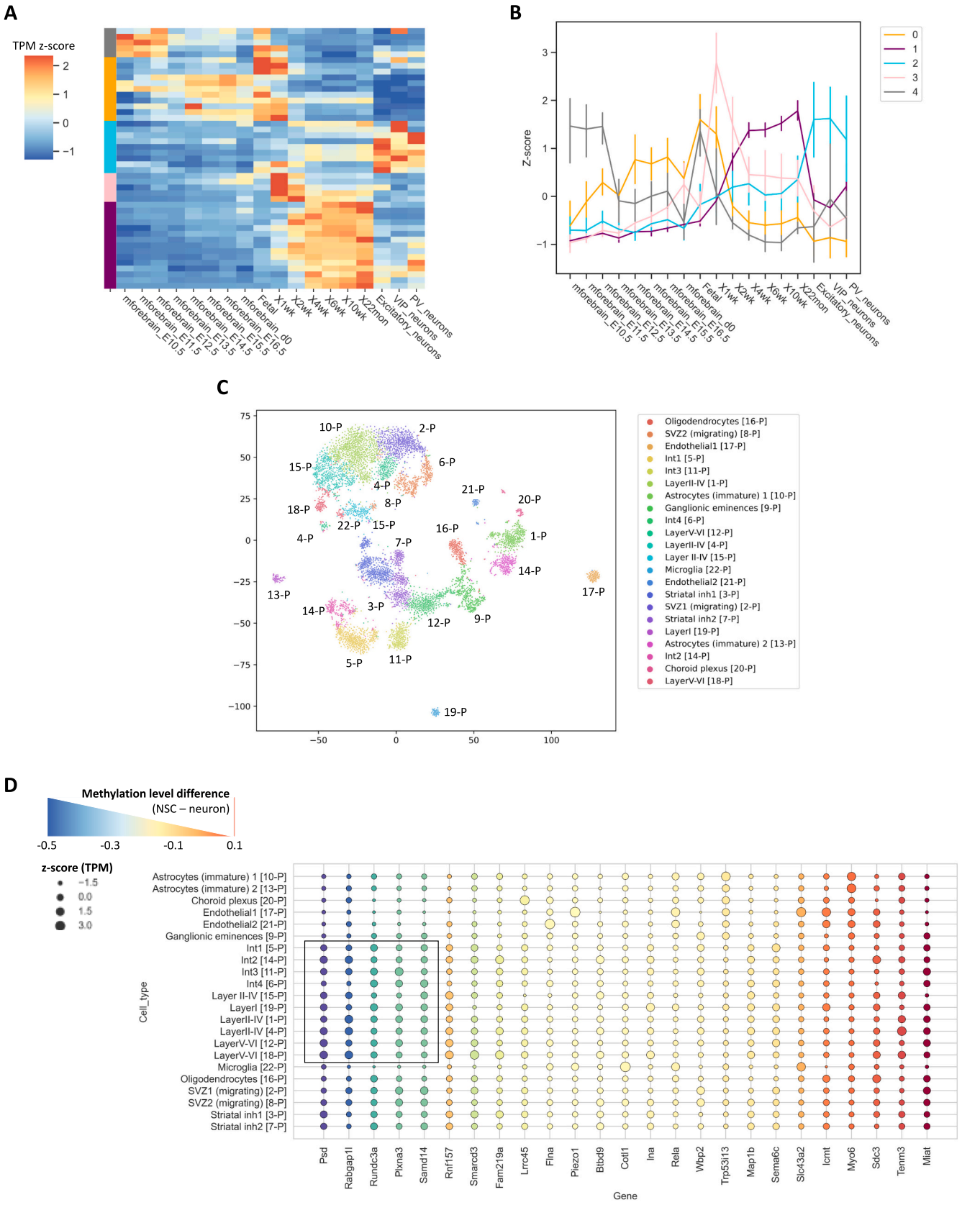

Fig. 6. Temporal and spatial expression of differentially methylated transcripts. (A) Clustering analysis of expression profiles for differentially methylated transcripts. *Z*-score of TPM was used to perform clustering. (B) Linear representation of clusters identified in (A). Error bars represent standard deviation. (A) and (B) share the same color code. (C) tSNE clustering of scRNAseq P0 brain tissue from Loo et al., 2019 [22]. p is denoted as postnatal. (D) TPM z-score of differentially methylated transcripts using scRNA-seq data generated for P0 brain. Color of bubble plot indicates methylation level differences between NSC and neuron RNA BS-seq samples.

these genes, such a cell-type predominant expression was also reported in previous studies. For example, localized expression of *Rundc3a* was previously found to be concentrated within noradrenergic populations of multiple brain regions [45,46]. Taken together, these results indicate that highly methylated transcripts in mature neuron populations have temporal and cell-type predominant expression patterns.

4. Discussion

Cytosine methylation of mRNA has emerged as a critical regulator of mRNA transportation, stability and translation [5,7,33,48,49]. Despite distinct mRNA methylation profiles reported in brain and NSCs [17], no attempt has been made to characterize mRNA m^5C methylation patterns in the developing mammalian brain. In this study, we provide both gene expression and mRNA cytosine methylation profiles for NSCs, mature neurons, and postnatal brain tissues.

RNA cytosine methylation profiling can be achieved with m^5C-specific antibodies to enrich methylated transcripts followed by deep-sequencing [50,51]. Such an approach has resolution limitations and is highly dependent on the quality of antibody used. Despite the fact that bisulfite sequencing remains the gold standard for RNA cytosine methylation detection, our recent experiments [27], together with reports from other labs [8,52], indicated that both experimental procedure and methylation calling have a significant impact on the detection of RNA methylation. Thus, inconsistent methylation sites may be observed between biological replicates. In this study, we found that high-confidence m^5C sites shared by two biological replicates tend to have a higher methylation level and more read coverage than those of low-confidence m^5C sites identified in one biological replicate only. In addition, low-confidence sites frequently reside in a transcript sensitive to bisulfite treatment.

Notwithstanding current technical challenges in the determination of RNA cytosine methylation, our analyses on high-confidence m^5C sites led to a few interesting findings. Consistent with previous studies [7,8,17], methylated cytosines are preferentially enriched around the translation initiation sites of mRNAs and usually have a methylation level between 20 and 30% with a downstream "GGG" motif. Approximately 6% of high-confidence m^5C sites identified in this study were methylated across all samples. However, the diversity of mRNA methylation increases in differentiated neurons. In addition, increased methylation in neurons were observed in 96% of the DMSs identified between NSCs *vs* neurons. Previous studies linked the methylation of both tRNA and mRNA to synapse formation [13,15]. Intriguingly, the DMSs identified in P17 *vs* P0 and 6 W brain tissues were significantly enriched for synaptic plasticity. This suggests that mRNA cytosine methylation may also play important roles during brain development.

In this study, we examined the expression profiles of RNA cytosine methylation readers, writers, and erasers. As a result of tRNA degradation, neuronal synapse function was impaired in the NSUN2 knockout mouse model [16]. Interestingly, most of the factors regulating m^5C methylation were downregulated during development in the comparison between P17 and P0 but showed no significant change in the comparison between 6 W and P17. This result suggests the highly dynamic regulation of mRNA m^5C methylation during early postnatal brain development, and it may reach homeostasis in the maturing brain. The integration of RNA-seq data with RNA BS-seq data allowed us to explore the correlation between the levels of gene expression and RNA methylation. A weak to moderate positive correlation was observed in general, but such a trend may not be true for all transcripts. This suggests that the regulation of RNA expression and methylation might be positively correlated and the methylated transcripts could be cell-type predominant, spatially, and/or temporally regulated. Future studies are needed to explore how cell-type predominant mRNA methylation may contribute to neuronal differentiation. Collectively, our study provided insight into the RNA m^5C methylation dynamics of the developing brain and is a rich resource to facilitate further investigation on the role of brain mRNA cytosine methylation.

Author contributions

H.X. conceived and designed the study; X.X. isolated and cultured E16.5 mouse cortical neurons and neural stem cells, constructed libraries for RNA-seq and RNA bisulfite sequencing; Z.J. and Y.L. performed the bioinformatic analyses; X.X., Z.J., Y.L., and H.X. interpreted results and wrote the manuscript. All authors have read and agreed to the published version of the manuscript.

Funding

This study was supported by NIH grant ES031521, NS094574, MH120498, NSF1922428, the Center for One Health Research at the Virginia-Maryland College of Veterinary Medicine and the Edward *Via* College of Osteopathic Medicine, the Center for Engineered Health, the Virginia-Maryland College of Veterinary Medicine at Virginia Tech, and the Fralin Life Sciences Institute faculty development fund for H.X.

Informed consent statement

Not applicable.

Declaration of Competing Interest

The authors declare no conflict of interest.

Data availability

Data will be made available on request.

Acknowledgments

We thank Dr. Janet Webster for English language editing.

Appendix A. Supplementary data

Supplementary data to this article can be found online at https://doi.org/10.1016/j.ygeno.2023.110604.

References

[1] X. Xu, X. Wei, H. Xie, Advances in methods and software for RNA cytosine methylation analysis, Genomics 112 (2020) 1840–1846.
[2] F. Tuorto, R. Liebers, T. Musch, M. Schaefer, S. Hofmann, S. Kellner, M. Frye, M. Helm, G. Stoecklin, F. Lyko, RNA cytosine methylation by Dnmt2 and NSun2 promotes tRNA stability and protein synthesis, Nat. Struct. Mol. Biol. 19 (2012) 900–905.
[3] M.D. Metodiev, H. Spahr, P. Loguercio Polosa, C. Meharg, C. Becker, J. Altmueller, B. Habermann, N.G. Larsson, B. Ruzzenente, NSUN4 is a dual function mitochondrial protein required for both methylation of 12S rRNA and coordination of mitoribosomal assembly, PLoS Genet. 10 (2014), e1004110.
[4] Y. Cámara, J. Asin-Cayuela, Metodi Chan, Y. Shi, B. Ruzzenente, C. Kukat, B. Habermann, R. Wibom, K. Hultenby, et al., MTERF4 regulates translation by targeting the methyltransferase NSUN4 to the mammalian mitochondrial ribosome, Cell Metab. 13 (2011) 527–539.
[5] Y. Yang, L. Wang, X. Han, W.L. Yang, M. Zhang, H.L. Ma, B.F. Sun, A. Li, J. Xia, J. Chen, et al., RNA 5-Methylcytosine facilitates the maternal-to-zygotic transition by preventing maternal mRNA decay, Mol. Cell 75 (6) (2019) 1188–1202.e11.
[6] J. Liu, T. Huang, W. Chen, C. Ding, T. Zhao, X. Zhao, B. Cai, Y. Zhang, S. Li, L. Zhang, et al., Developmental mRNA m5C landscape and regulatory innovations of massive m5C modification of maternal mRNAs in animals, Nat. Commun. (2022) 13.
[7] X. Yang, Y. Yang, B.F. Sun, Y.S. Chen, J.W. Xu, W.Y. Lai, A. Li, X. Wang, D. P. Bhattarai, W. Xiao, et al., 5-methylcytosine promotes mRNA export - NSUN2 as the methyltransferase and ALYREF as an m(5)C reader, Cell Res. 27 (2017) 606–625.
[8] T. Huang, W. Chen, J. Liu, N. Gu, R. Zhang, Genome-wide identification of mRNA 5-methylcytosine in mammals, Nat. Struct. Mol. Biol. 26 (2019) 380–388.
[9] L. Fu, C.R. Guerrero, N. Zhong, N.J. Amato, Y. Liu, S. Liu, Q. Cai, D. Ji, S.-G. Jin, L. J. Niedernhofer, et al., Tet-mediated formation of 5-Hydroxymethylcytosine in RNA, J. Am. Chem. Soc. 136 (2014) 11582–11585.

[10] J. Lan, N. Rajan, M. Bizet, A. Penning, N.K. Singh, D. Guallar, E. Calonne, A. Li Greci, E. Bonvin, R. Deplus, et al., Functional role of Tet-mediated RNA hydroxymethylcytosine in mouse ES cells and during differentiation, Nat. Commun. (2020) 11.
[11] H. Chen, H. Yang, X. Zhu, T. Yadav, J. Ouyang, S.S. Truesdell, J. Tan, Y. Wang, M. Duan, L. Wei, et al., m5C modification of mRNA serves a DNA damage code to promote homologous recombination, Nat. Commun. (2020) 11.
[12] Y. Yang, L. Wang, X. Han, W.L. Yang, M. Zhang, H.L. Ma, B.F. Sun, A. Li, J. Xia, J. Chen, et al., RNA 5-Methylcytosine facilitates the maternal-to-zygotic transition by preventing maternal mRNA decay, Mol. Cell 75 (1188–1202) (2019), e1111.
[13] S. Blanco, S. Dietmann, J.V. Flores, S. Hussain, C. Kutter, P. Humphreys, M. Lukk, P. Lombard, L. Treps, M. Popis, et al., Aberrant methylation of tRNAs links cellular stress to neuro-developmental disorders, EMBO J. 33 (2014) 2020–2039.
[14] S. Blanco, M. Frye, Role of RNA methyltransferases in tissue renewal and pathology, Curr. Opin. Cell Biol. 31 (2014) 1–7.
[15] J.V. Flores, L. Cordero-Espinoza, F. Oeztuerk-Winder, A. Andersson-Rolf, T. Selmi, S. Blanco, J. Tailor, S. Dietmann, M. Frye, Cytosine-5 RNA methylation regulates neural stem cell differentiation and motility, Stem Cell Reports 8 (2017) 112–124.
[16] J. Blaze, A. Navickas, H.L. Phillips, S. Heissel, A. Plaza-Jennings, S. Miglani, H. Asgharian, M. Foo, C.D. Katanski, C.P. Watkins, et al., Neuronal Nsun2 deficiency produces tRNA epitranscriptomic alterations and proteomic shifts impacting synaptic signaling and behavior, Nat. Commun. (2021) 12.
[17] T. Amort, D. Rieder, A. Wille, D. Khokhlova-Cubberley, C. Riml, L. Trixl, X.Y. Jia, R. Micura, A. Lusser, Distinct 5-methylcytosine profiles in poly(A) RNA from mouse embryonic stem cells and brain, Genome Biol. 18 (2017) 1.
[18] H. Jian, C. Zhang, Z. Qi, X. Li, Y. Lou, Y. Kang, W. Deng, Y. Lv, C. Wang, W. Wang, et al., Alteration of mRNA 5-Methylcytosine modification in neurons after OGD/R and potential roles in cell stress response and apoptosis, Front. Genet. 12 (2021), 633681.
[19] C.U. Awah, J. Winter, C.M. Mazdoom, O.O. Ogunwobi, NSUN6, an RNA methyltransferase of 5-mC controls glioblastoma response to temozolomide (TMZ) via NELFB and RPS6KB2 interaction, Cancer Biol. Therapy 22 (2021) 587–597.
[20] A.A. Dillman, M.R. Cookson, Transcriptomic Changes in Brain Development, Elsevier, 2014, pp. 233–250.
[21] L. Tan, W. Ma, H. Wu, Y. Zheng, D. Xing, R. Chen, X. Li, N. Daley, K. Deisseroth, X. S. Xie, Changes in genome architecture and transcriptional dynamics progress independently of sensory experience during post-natal brain development, Cell 184 (2021) 741–758.e717.
[22] L. Loo, J.M. Simon, L. Xing, E.S. McCoy, J.K. Niehaus, J. Guo, E.S. Anton, M. J. Zylka, Single-cell transcriptomic analysis of mouse neocortical development, Nat. Commun. (2019) 10.
[23] T.K. Hensch, Critical period plasticity in local cortical circuits, Nat. Rev. Neurosci. 6 (2005) 877–888.
[24] M.H. Theus, J. Ricard, D.J. Liebl, Reproducible expansion and characterization of mouse neural stem/progenitor cells in adherent cultures derived from the adult subventricular zone, Curr. Protoc. Stem Cell Biol. Chapter 2 (2012). Unit 2D.8.
[25] A.N. Malik, T. Vierbuchen, M. Hemberg, A.A. Rubin, E. Ling, C.H. Couch, H. Stroud, I. Spiegel, K.K. Farh, D.A. Harmin, M.E. Greenberg, Genome-wide identification and characterization of functional neuronal activity-dependent enhancers, Nat. Neurosci. 17 (2014) 1330–1339.
[26] Z. Sun, X. Xu, J. He, A. Murray, M.A. Sun, X. Wei, X. Wang, E. McCoig, E. Xie, X. Jiang, et al., EGR1 recruits TET1 to shape the brain methylome during development and upon neuronal activity, Nat. Commun. 10 (2019) 3892.
[27] Z. Johnson, X. Xu, C. Pacholec, H. Xie, Systematic evaluation of parameters in RNA bisulfite sequencing data generation and analysis, NAR Genom Bioinform 4 (2022) lqac045.
[28] D. Rieder, T. Amort, E. Kugler, A. Lusser, Z. Trajanoski, meRanTK: methylated RNA analysis ToolKit, Bioinformatics 32 (2016) 782–785.
[29] B. Li, C.N. Dewey, RSEM: accurate transcript quantification from RNA-Seq data with or without a reference genome, BMC Bioinform. 12 (2011) 323.
[30] M.I. Love, W. Huber, S. Anders, Moderated estimation of fold change and dispersion for RNA-seq data with DESeq2, Genome Biol. 15 (2014) 550.
[31] D.W. Huang, B.T. Sherman, Q. Tan, J.R. Collins, W.G. Alvord, J. Roayaei, R. Stephens, M.W. Baseler, H.C. Lane, R.A. Lempicki, The DAVID gene functional classification tool: a novel biological module-centric algorithm to functionally analyze large gene lists, Genome Biol. 8 (2007) R183.
[32] Z. Zhang, T. Chen, H.X. Chen, Y.Y. Xie, L.Q. Chen, Y.L. Zhao, B.D. Liu, L. Jin, W. Zhang, C. Liu, et al., Systematic calibration of epitranscriptomic maps using a synthetic modification-free RNA library, Nat. Methods 18 (2021) 1213–1222.
[33] U. Schumann, H.N. Zhang, T. Sibbritt, A. Pan, A. Horvath, S. Gross, S.J. Clark, L. Yang, T. Preiss, Multiple links between 5-methylcytosine content of mRNA and translation, BMC Biol. 18 (2020) 40.
[34] H. Ahlenius, S. Chanda, A.E. Webb, I. Yousif, J. Karmazin, S.B. Prusiner, A. Brunet, T.C. Südhof, M. Wernig, FoxO3 regulates neuronal reprogramming of cells from postnatal and aging mice, Proc. Natl. Acad. Sci. 113 (2016) 8514–8519.
[35] M.C.H. Boersma, E.C. Dresselhaus, L.M. De Biase, A.B. Mihalas, D.E. Bergles, M. K. Meffert, A requirement for nuclear factor- B in developmental and plasticity-associated synaptogenesis, J. Neurosci. 31 (2011) 5414–5425.
[36] J. Wright, R.A. Kahn, E. Sztul, Regulating the large Sec7 ARF guanine nucleotide exchange factors: the when, where and how of activation, Cell. Mol. Life Sci. 71 (2014) 3419–3438.
[37] J.-C. Deloulme, S. Gory-Fauré, F. Mauconduit, S. Chauvet, J. Jonckheere, B. Boulan, E. Mire, J. Xue, M. Jany, C. Maucler, et al., Microtubule-associated protein 6 mediates neuronal connectivity through Semaphorin 3E-dependent signalling for axonal growth, Nat. Commun. 6 (2015) 7246.
[38] C. Cuveillier, J. Delaroche, M. Seggio, S. Gory-Fauré, C. Bosc, E. Denarier, M. Bacia, G. Schoehn, H. Mohrbach, I. Kulić, et al., MAP6 is an intraluminal protein that induces neuronal microtubules to coil, Sci. Adv. 6 (2020) eaaz4344.
[39] A. Hienola, S. Tumova, E. Kulesskiy, H. Rauvala, N-syndecan deficiency impairs neural migration in brain, J. Cell Biol. 174 (2006) 569–580.
[40] Y.-P. Hsueh, M. Sheng, Regulated expression and subcellular localization of Syndecan Heparan sulfate proteoglycans and the Syndecan-binding protein CASK/LIN-2 during rat brain development, J. Neurosci. 19 (1999) 7415–7425.
[41] L. Trixl, A. Lusser, The dynamic RNA modification 5-methylcytosine and its emerging role as an epitranscriptomic mark, Wiley Interdiscip. Rev. RNA 10 (2019), e1510.
[42] K.E. Bohnsack, C. Hobartner, M.T. Bohnsack, Eukaryotic 5-methylcytosine (m(5)C) RNA methyltransferases: mechanisms, cellular functions, and links to disease, Genes (Basel) (2019) 10.
[43] Y. Motorin, F. Lyko, M. Helm, 5-methylcytosine in RNA: detection, enzymatic formation and biological functions, Nucleic Acids Res. 38 (2010) 1415–1430.
[44] R. Garcia-Vilchez, A. Sevilla, S. Blanco, Post-transcriptional regulation by cytosine-5 methylation of RNA, Biochim. Biophys. Acta Gene Regul. Mech. 1862 (2019) 240–252.
[45] E. Sjöstedt, W. Zhong, L. Fagerberg, M. Karlsson, N. Mitsios, C. Adori, P. Oksvold, F. Edfors, A. Limiszewska, F. Hikmet, et al., An atlas of the protein-coding genes in the human, pig, and mouse brain, Science 367 (2020) eaay5947.
[46] M. Uhlén, L. Fagerberg, B.M. Hallström, C. Lindskog, P. Oksvold, A. Mardinoglu, Å. Sivertsson, C. Kampf, E. Sjöstedt, A. Asplund, et al., Tissue-based map of the human proteome, Science 347 (2015) 1260419.
[47] A. Buniello, N.J. Ingham, M.A. Lewis, A.C. Huma, R. Martinez-Vega, I. Varela-Nieto, G. Vizcay-Barrena, R.A. Fleck, O. Houston, T. Bardhan, et al., Wbp2 is required for normal glutamatergic synapses in the cochlea and is crucial for hearing, EMBO Mol. Med. 8 (2016) 191–207.
[48] X. Chen, A. Li, B.F. Sun, Y. Yang, Y.N. Han, X. Yuan, R.X. Chen, W.S. Wei, Y. Liu, C. C. Gao, et al., 5-methylcytosine promotes pathogenesis of bladder cancer through stabilizing mRNAs, Nat. Cell Biol. 21 (2019) 978–990.
[49] X. Xu, Z. Johnson, A. Wang, R.L. Padget, J.W. Smyth, H. Xie, Folate regulates RNA m(5)C modification and translation in neural stem cells, BMC Biol. 20 (2022) 261.
[50] X. Cui, Z. Liang, L. Shen, Q. Zhang, S. Bao, Y. Geng, B. Zhang, V. Leo, L.A. Vardy, T. Lu, et al., 5-methylcytosine RNA methylation in *Arabidopsis Thaliana*, Mol. Plant 10 (2017) 1387–1399.
[51] S. Edelheit, S. Schwartz, M.R. Mumbach, O. Wurtzel, R. Sorek, Transcriptome-wide mapping of 5-methylcytidine RNA modifications in bacteria, archaea, and yeast reveals m5C within archaeal mRNAs, PLoS Genet. 9 (2013), e1003602.
[52] C. Legrand, F. Tuorto, M. Hartmann, R. Liebers, D. Jacob, M. Helm, F. Lyko, Statistically robust methylation calling for whole-transcriptome bisulfite sequencing reveals distinct methylation patterns for mouse RNAs, Genome Res. 27 (2017) 1589–1596.